energies

MDPI

Article

Application of Phase Change Material-Based Thermal Capacitor in Double Tube Heat Exchanger—A Numerical Investigation

Matthew Fong [1], Jundika Kurnia [2] and Agus P. Sasmito [1,*,†]

[1] Department of Mining and Materials Engineering, McGill University, Montreal, QC H3A 2A7, Canada; mathew.fong@mail.mcgill.ca

[2] Department of Mechanical Engineering, Universiti Teknologi PETRONAS, Seri Iskandar 32610, Malaysia; jundika.kurnia@utp.edu.my

* Correspondence: agus.sasmito@mcgill.ca; Tel.: +1-514-398-3788

† Current address: 115-3450 University Street, Montreal, QC H3A 0E8, Canada.

Received: 5 July 2020; Accepted: 14 August 2020; Published: 20 August 2020

Abstract: In many heat transfer related applications, there is a need for a stable, constant supply temperature. As a result, the integration of intermittent renewable sources of heat into these processes can prove to be challenging, requiring special temperature smoothing devices or strategies. This study focuses on the application of phase change materials integrated into a double tube heat exchanger as a possible thermal smoothing device. The objective of this study is to evaluate the ability of the exchanger to smoothen out temperature variations within the cold stream outlet while the hot stream is subject to oscillating inlet conditions. A computational fluid dynamics approach is used where a numerical model is developed, validated and then used to model the conjugate heat transfer within the heat exchanger. Four organic phase change materials (PCM) with different phase change temperatures were selected for investigation (myristic, octadecane, eicosane, and wax) to study the relationship between melting temperature and stabilization performance. A parametric study was then conducted by varying the Reynolds number of the flow as well as temperature oscillation period and amplitude to study the sensitivity of the system. The results confirm the potential of a phase change material-based thermal capacitor at dampening oscillations across the heat exchanger.

Keywords: thermal capacitor; phase change material; latent heat; thermal storage; thermal smoothening; energy storage

1. Introduction

In many industrial processes maintaining a constant temperature is crucial for operations, in particular, to ones with stringent temperature requirements. With the interest in reducing emissions, the inclusion of renewable heat sources or recovered process heat has garnered considerable interest [1]. Under these conditions, however, fluctuations in supply temperature are to be expected, for example, when using solar collectors supply temperature will vary with solar irradiation or when recovering heat from an intermittent process [2]. Therefore, a method of supply temperature regulation that can provide stable output despite fluctuations in the input temperature is needed. One promising strategy is to incorporate a thermal capacitor or stabilizer upstream of any temperature sensitive process. Thermal capacitors possess the ability to reduce fluctuations in temperature by absorbing and releasing thermal energy as needed to smoothen out energy demand [3]. There are two types of thermal capacitors: active thermal capacitors, where storage is actively managed, requiring additional energy input to control temperature and passive thermal capacitors which use passive media to control the heat transfer such as a large thermal mass [3]. This thermal mass can use either sensible or latent

heat storage for stabilization. In the case of sensible heat storage, their changing temperature may have adverse effects on thermal stability as their temperature increases and decreases with the amount of heat stored. Latent heat thermal storage comprised of phase change materials (PCMs) can absorb large amounts of energy at constant temperature [4,5], making them an excellent candidate for thermal stabilization. However, to achieve an optimum thermal capacitor design using PCMs, comprehensive knowledge and expertise of the fluid flow and heat transfer process between the heat transfer fluid and phase change materials inside the thermal capacitor is crucial.

Unfortunately, while studies of PCMs as energy storage media are abundantly available, there are fewer studies on the application of PCMs as thermal capacitors. Furthermore, most studies on the use of PCMs as thermal capacitors or regulators have been predominantly focused on applications within space heating/cooling or electronic devices with a few studies focusing on industrial heat processes. Among the studies on industrial processes, Verdier et al. [6] performed one where a thermal energy storage device was connected to a solar receiver to stabilize the outlet air temperature. The air was used to supply a combustion chamber of a hybrid solar gas turbine power plant, active controls were used to manage energy storage and recovery from the PCM based on the detected temperature coming from the solar receiver. Nardin et al. [7] proposed a new system exploiting a PCM to reduce the fluctuation of off-gas temperature to achieve efficient energy recovery from an electric arc furnace. The off-gas was directed to flow over a series of tubes containing PCM; they found that as a result, the temperature of the off-gas was stabilized significantly, thus allowing for the use of a Rankine-based heat recovery system. In a follow-up study [2], the same authors extended the system for continuous energy recovery from the electric arc furnace. In the new study, they found that the temperature fluctuations from the recovered gas had been greatly stabilized which led to an increase in the efficiency of their recovery system. Furthermore, they investigated the effect of thermal stress of their proposed system [8] and added an auxiliary section which provided the heat required for leveling the thermal content of the off-gas [9]. Alawadhi et al. [10] used a phase change material to smoothen temperature variations of a fluid flowing in a channel and showed that by using the PCM as a thermal capacitor, large swings in temperature at the inlet could be dampened at the outlet. Charvat et al. [11] studied the suitability for a water-PCM heat exchanger to act as a thermal stabilizer. They conducted experiments which used square-wave temperature fluctuations at the water inlet and concluded that effective temperature stabilization was possible when the inlet temperature fluctuated around the phase change temperature of the PCM. In another study, Charvat et al. [12] numerically compared sensible-based and latent heat-based thermal capacitors. The study used two materials for sensible heat (copper and concrete) and two materials for latent heat storage (octadecane and calcium chloride hexahydrate). The authors found that latent heat-based storage materials had better results in smoothing temperature fluctuations as compared to the sensible heat storage system in the cases where the fluctuations occurred around the phase change temperature of the PCMs. In a previous study by the present authors [13], a PCM thermal capacitor that used a simple tube flow was numerically investigated. Results showed that temperature fluctuations at the outlet were reduced and that the introduction of fins into the PCM could be used to improve dampening.

To develop a better understanding of the application of PCMs as thermal capacitors, the present study is conducted to numerically investigate the performance of a triplex heat exchanger with an integrated PCM. Previous authors studied this configuration at larger scales and demonstrated that is well suited for use as a thermal energy storage device [14]. The scope of this study is first limited to the laminar regime to better understand the possible temperature gradients that can be generated from the system. The inclusion of turbulence and the practical considerations within a heat exchanger system are left for further studies as they introduce other avenues of investigation. To generate fluctuations at the hot stream inlet, a sinusoidal temperature profile with constant fluid velocity is set at the inlet of the hot stream. The performance of the thermal capacitor is evaluated by analyzing the change in the magnitude of the fluctuation amplitude of the outlet temperature and comparing it to a case without the integrated phase change material. To evaluate the effect of PCM melting temperature

on performance, four organic PCMs (octadecane, eicosane, wax, and myristic acid) are evaluated. The effect of fluid inlet Reynolds number, oscillation amplitude and oscillation period were also investigated for their effect on system performance.

This paper progresses by first presenting the relevant governing equations followed by the material properties and boundary conditions. The computational procedure is then presented along with details of model validation. The results section is split into three parts; the first part details the selection of the flow configuration, the second details the results from a base case and the third present the results from variations in Reynolds, oscillation range and period.

2. Mathematical Model

A two dimensional axisymmetric computational fluid dynamics (CFD) model was used to analyze the performance of the thermal capacitor. The model consisted of three nested tubes with the inner tube containing the hot stream, the outer tube containing the cold stream and the middle tube containing the PCM as illustrated in Figure 1. Detailed geometric parameters of the studied case are summarized in Table 1 along with a detailed drawing in Figure 1. The hot stream inlet temperature was set to a constant flow rate with a fluctuating temperature boundary condition while the inlet temperature of the cold stream was held constant. The PCMs considered in this study were n-octadecane, n-eicosane, myristic acid and a paraffin wax while the heat transfer fluid (HTF) used was water.

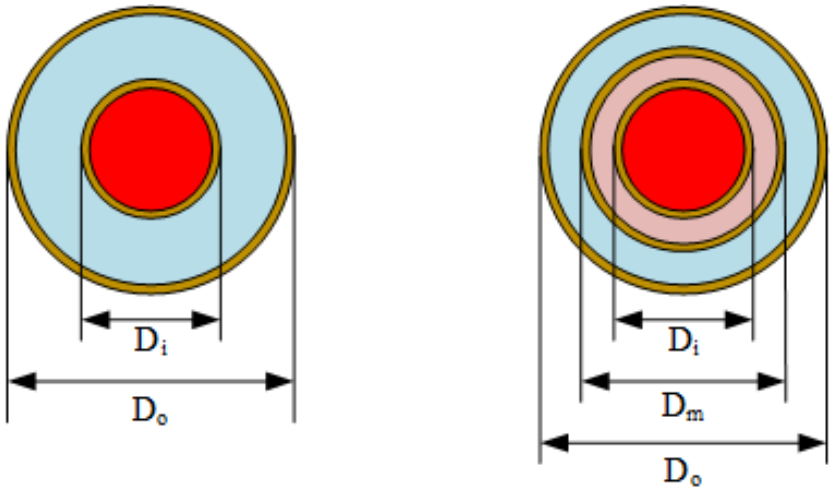

Figure 1. Cross section schematic of double pipe heat exchanger with and without PCM thermal capacitor.

Table 1. Geometric parameters of heat exchanger.

Parameters	Value	Unit	Description
D_i	3.00×10^{-2}	m	diameter of inner pipe
D_m	4.00×10^{-2}	m	diameter of phase change pipe
D_o	5.66×10^{-2}	m	diameter of outer pipe
Z	2	m	length of heat exchange domain

2.1. Governing Equations

A mathematical model is formulated into three zones: two zones containing the flowing heat transfer fluid and one zone containing the phase change material. The problem is reduced to a 2D axis-symmetric simulation with no internal heat generation, negligible heat generated by viscous dissipation and laminar flow conditions. Conservation of mass, energy and momentum are solved with the zones being thermally coupled together. Numerics were validated previously by Kurnia et al. [15–17] for a latent heat thermal energy storage system and additional verification steps

were performed for the model reduction and are presented in Section 3. The conservation equations for three regions are as follows:

2.1.1. Heat Transfer in the Heat Transfer Fluid

Conservation equation of mass:

$$\frac{\partial \rho_{htf}}{\partial t} + \nabla \cdot (\rho_{htf} \mathbf{U}) = 0 \tag{1}$$

Conservation equation of momentum:

$$\frac{\partial \left(\rho_{htf} \mathbf{U}\right)}{\partial t} + \nabla \cdot \left(\rho_{htf} \mathbf{U}\mathbf{U}\right) = -\nabla p + \nabla \cdot \left(\mu_{htf} \left(\nabla \mathbf{U} + (\nabla \mathbf{U})^T\right)\right) \tag{2}$$

Conservation equation of energy:

$$\frac{\partial \left(\rho_{htf} h_{htf}\right)}{\partial t} + \nabla \cdot \left(\rho_{htf} h_{htf} \mathbf{U}\right) = \nabla \cdot (k \nabla T) \tag{3}$$

2.1.2. Heat Transfer in the Wax

To account for the phase change of the PCM, a volume averaged enthalpy-porosity formulation of the energy equation is adopted.

- Conservation equation of mass:

$$\frac{\partial \rho_{pcm}}{\partial t} + \nabla \cdot (\rho_{pcm} \mathbf{U}) = 0 \tag{4}$$

- Conservation equation of momentum:

$$\frac{\partial \left(\rho_{pcm} \mathbf{U}\right)}{\partial t} + \nabla \cdot \left(\rho_{pcm} \mathbf{U}\mathbf{U}\right) = \nabla \cdot (\mu \nabla \mathbf{U}) - \nabla p - \underbrace{\mathbf{U} C_m \frac{(1-\gamma)^2}{\gamma^3}}_{S_M} \tag{5}$$

where γ is the liquid fraction and S_M is the mushy term which is used to control movement in the PCM during phase change. When $\gamma = 1$ the PCM is fully liquid and the term disappears. When $\gamma = 0$ and the PCM is fully solidified the source term becomes very large due to the division, which requires that velocity be forced to zero in order satisfy the equation.

- Conservation equation of energy:

$$\begin{gathered} \frac{\partial}{\partial t}[(\gamma \rho_{pcm,l} h_l + (1-\gamma)\rho_{pcm,s} h_s)] + \nabla \cdot (\rho_{pcm,l} h_l \mathbf{U}) = \\ \nabla \cdot (k_e \nabla T) - \underbrace{\left[\left(\rho_{pcm,l} \Delta H \frac{\partial \gamma}{\partial t}\right) + \Delta H \nabla \cdot (\rho_{pcm,l} \mathbf{U} \gamma)\right]}_{\text{Enthalpy of Phase Change}} \end{gathered} \tag{6}$$

2.2. Constitutive Relations

2.2.1. Properties of Water

Due to its temperature dependence, thermophysical properties of water are represented as polynomial functions of temperature as follows [18]

$$\rho_{htf} = C_{r,htf1} T^2 - C_{r,htf2} T + C_{r,htf3} \tag{7}$$

$$\mu_{htf} = C_{\mu,htf1} \times 10^{\frac{C_{\mu,htf2}}{T - C_{\mu,htf3}}} \tag{8}$$

$$k_{htf} = C_{k,htf1} T^2 + C_{k,htf2} T + C_{k,htf3} \tag{9}$$

where $C_{r,htf1}$, $C_{r,htf2}$, $C_{r,htf3}$, $C_{\mu,htf1}$, $C_{\mu,htf2}$, $C_{\mu,htf3}$, $C_{k,htf1}$, $C_{k,htf2}$, and $C_{k,htf3}$ are constants whose value are summarized in Table 2 Constant specific heat of 4200 J/(kg K) is specified. These properties were obtained from Kays et al. [19] and are applicable for temperatures ranging within 298 K and 373 K.

Table 2. Fitting constants for water material characteristic functions.

Parameters	Value	Unit
$C_{r,htf1}$	-3.57×10^{-3}	kg m^{-3} K^{-2}
$C_{r,htf2}$	1.88	kg m^{-3} K^{-1}
$C_{r,htf3}$	753.2	kg m^{-3}
$C_{\mu,htf1}$	2.591×10^{-5}	kg m^{-1} s^{-1}
$C_{\mu,htf2}$	238.3	K
$C_{\mu,htf3}$	143.2	K
$C_{k,htf1}$	-8.354×10^{-6}	W m^{-1} K^{-3}
$C_{k,htf2}$	6.53×10^{-3}	W m^{-1} K^{-2}
$C_{k,htf3}$	-0.5981	W m^{-1} K^{-1}
$c_{p,htf}$	4200	J kg^{-1} K^{-1}

2.2.2. Properties of PCM

In similar fashion to the authors' previous studies [15–17], the PCM properties are represented by

$$\rho_{pcm} = \frac{C_{\rho,pcm}}{C_\beta (T - T_l)} \tag{10}$$

$$k_{pcm} = \begin{cases} k_{s,pcm} & \text{if } T < T_s \\ k_{l,pcm} & \text{if } T \geq T_l \end{cases} \tag{11}$$

$$\mu_{pcm} = C_{\mu,pcm1} e^{\left(C_{\mu,pcm2} + \frac{C_{\mu,pcm3}}{T}\right)} \tag{12}$$

where $C_{\rho,pcm1}$, $C_{\mu,pcm1}$, $C_{\mu,pcm2}$, and $C_{\mu,pcm3}$ are constants, C_β is the PCMs thermal expansion coefficient, $k_{s,pcm}$ and $k_{l,pcm}$ are the PCMs thermal conductivity in the solid and liquid phase. Constant specific heats were specified for the various PCMs. Properties of the considered PCMs were taken from Hale et al. [20] and from previous work by Kurnia et al. [17] and are summarized in Table 3.

Table 3. Fitting constants for PCM material characteristic functions.

$c_{p,pcm}$	2160 (n-octadecane) 2210 (n-eicosane) 1590 (myristic acid) 2890 (wax)	J kg^{-1}K^{-1}
T_s, T_l	300.15, 300.65 (n-octadecane) 309.15, 309.65 (n-eicosane) 331.15, 331.65 (myristic acid) 319.15, 320.65 (wax)	K
$k_{s,pcm}$	0.358 (n-octadecane) 0.358 (n-eicosane) 0.365 (myristic acid) 0.321 (wax)	W m^{-1}K^{-1}
$k_{l,pcm}$	0.148 (n-octadecane) 0.148 (n-eicosane) 0.159 (myristic acid) 0.120 (wax)	W m^{-1}K^{-1}
$C_{\mu,pcm1}$	0.001	kg m^{-1}s^{-1}
$C_{\mu,pcm2}$	−4.649 (n-octadecane) −4.300 (n-eicosane) −4.659 (myristic acid) −4.250 (wax)	-
$C_{\mu,pcm3}$	1.790×10^3	K
L	2.43×10^5 (n-octadecane) 2.47×10^5 (n-eicosane) 1.99×10^5(myristic acid) 1.73×10^5(wax)	J kg^{-1}
$C_{\rho,pcm1}$	774 (n-octadecane) 778 (n-eicosane) 860 (myristic acid) 750 (wax)	kg m^{-3}
C_β	9.00×10^{-4}	K^{-1}

2.3. Initial and Boundary Conditions

The boundary conditions used for the model were as follows:

At the inlet of the hot stream a constant velocity corresponding to Reynolds numbers from 200 to 2000 in increments of 200 were specified and are reported in Table 5, velocity for the annular section was calculated by matching the mass flow rate of the inner pipe. Temperature of the inlet was controlled according to a sinusoidal fluctuating temperature as defined below. Other boundary conditions are reported in Table 4.

Table 4. Base case boundary conditions and parameters.

Parameters	Value	Unit
T_{mean}, T_{amp}	313.15, 20	K
$T_{c,in}$	293.15	K
P_{out} (gauge)	0	Pa
τ	600	s

$$\mathbf{U} = \mathbf{U_{in}}, T = T_{h,in} = T_{avg} - T_{amp} \cos\left(2\pi \frac{t}{\tau}\right) \quad (13)$$

Constant temperature and flow were defined at the inlet of the cold stream. The velocity of the cold stream was set such that the mass flow rate of water was the same as that in the hot stream and is reported in Table 5.

$$\dot{m} = \dot{m_{in}}, T = T_{c,in} \tag{14}$$

At the wall between the hot stream and the PCM, a no-slip condition was specified with a coupled wall. Similarly, the wall between the cold stream and the PCM was specified as no-slip and with coupled heat transfer.

$$\mathbf{U} = 0, T_{htf}|_{r=D_{i-}} = T_{pcm}|_{r=D_{i+}} \tag{15}$$

$$\mathbf{U} = 0, T_{htf}|_{r=D_{m-}} = T_{pcm}|_{r=D_{m+}} \tag{16}$$

The outer wall and the sidewall of the PCM container were specified as insulated walls with no-slip conditions imposed.

$$\mathbf{U} = 0, n \cdot \nabla(k_{htf} \nabla T) = 0|_{r=D_o} \tag{17}$$

The outlets were specified to be at zero gauge pressure with zero heat diffusion.

$$p = p_{out}, n \cdot \nabla(k_{htf} \nabla T) = 0 \tag{18}$$

Table 5. Inlet velocity boundary condition for hot and cold streams.

Reynolds Number	Inner (m/s)	Annulus (m/s)
200	0.0044	0.00246
400	0.0088	0.00493
600	0.0132	0.00740
800	0.0176	0.00987
1000	0.0219	0.01234
1200	0.0263	0.01481
1400	0.0307	0.01727
1600	0.0351	0.01974
1800	0.0395	0.02221
2000	0.0439	0.02468

3. Computational Procedure

The domain was reduced to a 2D axisymmetric model as the tangential components of heat transfer and flow were negligible. The inlets of the cold and hot stream were numerically extended by two meters with adiabatic heat transfer conditions to ensure that all cases were compared with fully developed flow. Phase change was modeled using the enthalpy porosity method and a user-defined function was used to implement the temperature dependent properties of the PCMs, water and the time dependent inlet temperature. The model was solved using ANSYS (17.2 Canonsburg, PA, USA) with second order discretization, time stepping of 0.5 s and convergence criteria of relative residuals set to 10^{-5}. The numerical model was validated previously by the authors and specific details can be found in Kurnia et al. [15]. Experimental results were taken from a study by Lacroix [21] in which the temperature within an annular PCM section were taken at two different points; results from the validation are shown in Figure 2.

A grid independence study was conducted to determine the appropriate number of elements for the domain. The study was conducted using one of the base cases for temperature oscillation and Reynolds number with grids varying from 120 k to 5000 k elements. No appreciable change was seen between the grids and 300 k element grid was selected to balance performance and independence. Similarly a temporal independence study was conducted and found no appreciable differences between time steps thus a time stepping of 0.5 s was chosen.

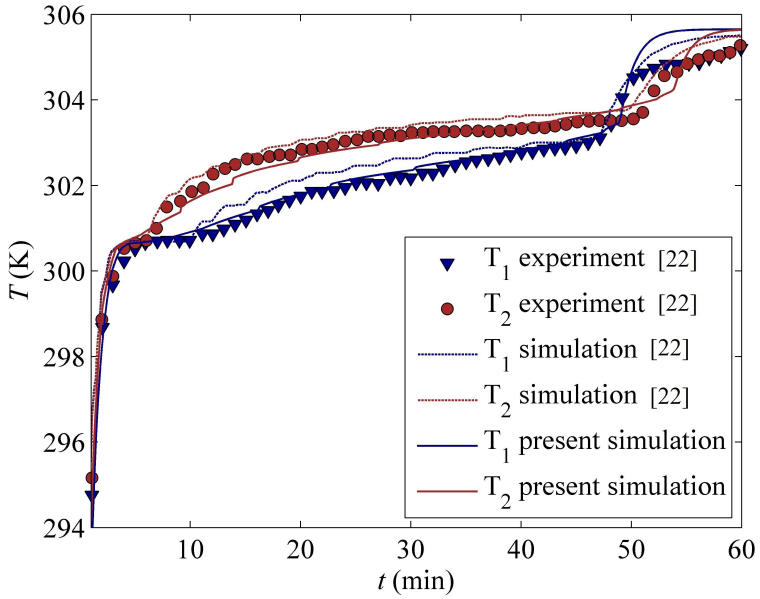

Figure 2. Validation of numerical model with experiments [15].

The contribution of natural convection to the overall heat transfer of the system was evaluated numerically. A 3D simulation including buoyancy driven natural convection in the PCM inner sleeve was run and the results compared to those of the 2D axisymmetric model as shown in Table 6. From the results it can be seen that the discrepancy or error of the 2D axisymmetric model was small. This is due to the presence of natural convection in only a small portion of the heat exchanger where sufficient PCM has melted to allow for natural convection to occur. Based on the counterflow configuration of the heat exchanger, only the section closest to the hot inlet is fully melted with the melted region thinning out further towards the cold inlet of the exchanger. This results in a minimal effect on overall heat transfer due to natural convection.

Table 6. Comparison of results with and without natural convection enabled.

	2D	3D (Convective)	% Error
Annulus Inlet Temp (K)		293.15	
Inner Inlet Temp (K)		313.15	
Bulk Annulus Temperature (K)	293.49	294.01	0.18%
Bulk Inner Temperature (K)	312.52	311.74	0.25%
Bulk PCM Temperature (K)	300.25	300.30	0.02%
PCM Liquid Fraction	0.3077	0.3128	1.63%
Flux Through PCM (W)	121.11	119.69	1.19%

4. Results and Discussion

The computational simulations were carried out for steady flow with a fluctuating temperature at the hot stream inlet. Both double pipe heat exchanger with and without PCM thermal capacitor were evaluated and discussed in light of numerical results. All cases were solved to steady state with a constant hot inlet temperature of 313.15 K before the oscillations were begun.

4.1. Selection of Flow Configuration

An initial study was performed to select the flow configuration of the exchanger; two cases were established as illustrated in Figure 3: Case A where the inner pipe was used for the hot stream and Case B where the inner pipe was used for the cold stream. The cases were run from Reynolds of 1400 to 2000 using a temperature amplitude of 20 K and a period of 10 min. The results are presented

in Figure 4 showing the average cold stream outlet temperature and oscillation range at different Reynolds numbers for each PCM and configuration. The results show that the average temperature for Case B was, in general, higher for all the PCMs and Reynolds numbers; however, fluctuations were higher. The Case A configuration was selected as it provided better overall thermal stabilization for the highest number of PCMs under study.

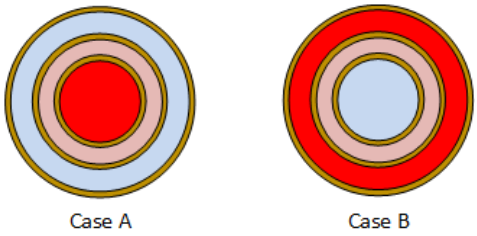

Figure 3. Case A and Case B configuration of hot and cold streams within the triplex heat exchanger.

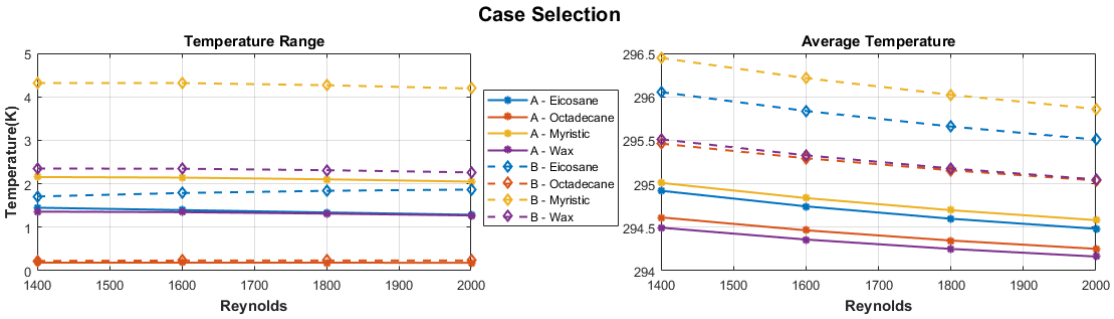

Figure 4. Cold outlet temperature fluctuation range and average temperature at various Reynolds numbers for different PCMs in Case A (hot inner) and Case B (cold inner) configuration.

4.2. Base Results

To evaluate the effectiveness of the thermal capacitor at smoothening out temperature variations, a base case was established and run with and without the inclusion of PCM at a Reynolds of 1000 with a 20 min period of oscillation and temperature amplitude of 20 K. Figure 5 shows the results from using four different PCMs to investigate the effect of different phase change temperatures (PCT). The PCMs were selected with different PCTs with n-octadecane, n-eicosane, myristic and the paraffin wax with PCTs of 301.65 K, 309.65 K, 331.65 K, and 319.15 K, respectively. From the results several features are apparent: the variations in the cold outlet temperatures are substantially reduced in the PCM cases although with a sizable decrease in the outlet average temperature. Among the PCMs, n-octadecane has the most stable outlet temperature followed by n-eicosane, paraffin wax and finally the myristic acid. The myristic and n-eicosane on inspection show a slightly higher average outlet temperature. The case with no PCM has an average temperature of 297.66 K with a range of 4.59 K, whereas the average temperatures for the PCM capacitor streams range from 294.91 K to 295.54 K with dampened ranges varying between 0.17 K to 1.99 K. Overall n-eicosane, myristic acid, n-octadecane and paraffin wax produce a 67%, 57%, 96% and 73% reduction in temperature oscillation with a corresponding reduction in average temperature of the cold stream by 49%, 47%, 58%, and 61%. These results demonstrate the ability for the PCM to act as a thermal capacitor with the ability to smoothen out the outlet temperature at the cost of less heat being transferred to the cold stream. Notably, the effect of different melting temperatures can be seen as fluctuations are reduced with decreasing phase change temperature. The reduced average temperature of the cold outlet as compared to the case with no PCM can be attributed to the presence of the phase change material. This is due to a combination of a decrease thermal diffusivity of the material limiting the rate of heat transfer as well as the phase change material transferring heat back into the hot stream. When energy is absorbed by the PCM it must be transferred through the PCM before it can be transferred to the cold stream. As the inlet

temperature oscillates the temperature of the hot stream periodically drops below that of the PCM layer and heat is transfered back into the hot stream as well as the cold stream. This does not occur for the no PCM case as the heat is transferred directly into the cold stream and the oscillation of the hot stream temperature never drop below that of the cold stream.

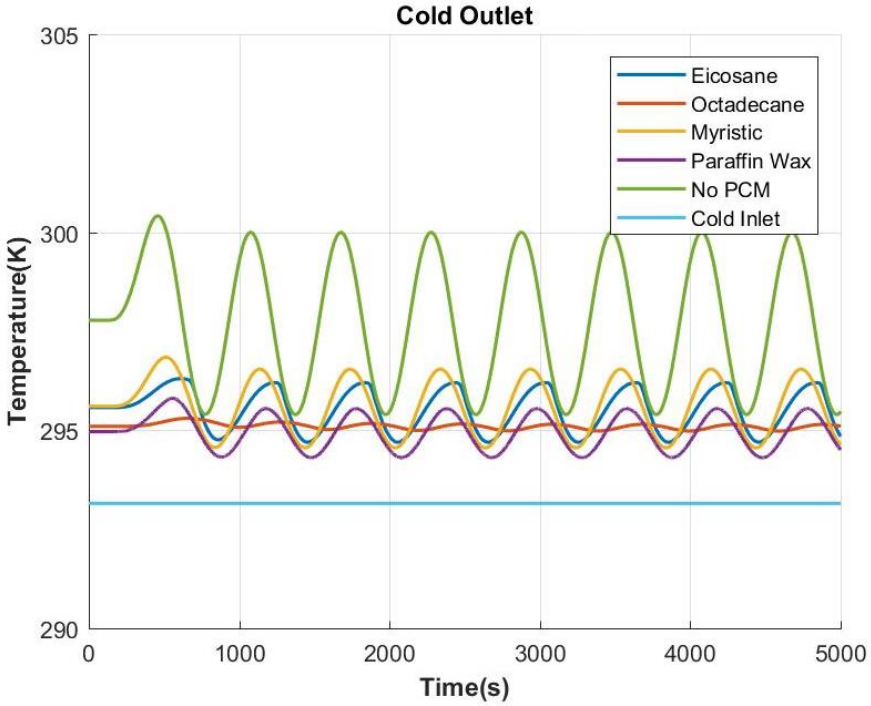

Figure 5. Cold outlets for base case and thermal capacitor cases with four PCMs at Re = 1000, cold inlet temperature is present to show the absolute temperature changes

4.3. Variation in Reynolds Number

The effect of changing flow velocity on the PCMs dampening capacity is examined by varying the Reynolds numbers of the hot stream from 200, 400, 600, 800, 1000, 1200, 1400, 1600, 1800 and 2000. The results are summarized in Figures 6–9, showing the liquid fraction activity and outlet temperature of the cold stream. A summary of oscillation range and mean temperature by Reynolds number is also shown in Figure 10. One common result that can be seen between the different PCMs at different Reynolds is the strong dampening which occurs at very low Reynolds numbers. This is caused due to the numerical extension that was added to the pipe in order to create the a fully developed velocity profile at the inlet. As a result as the temperature fluctuates over time, because of the lengths and speeds involved, the advection is much stronger in the free stream and slower along the wall resulting in a temperature gradient that is temporarily linked, for example the fluid in the free stream was injected 30 s before what is traveling along the wall. This effect becomes less pronounced as the Reynolds number increases and is less significant after a Reynolds of 1000. It is expected that this property would be absent for turbulent flows due to the turbulent mixing occurring across the flow but is present because of the very low velocities this study.

From Figure 6 it can be seen that as Reynolds number increases the average temperature decreases with the largest change seen when going from a Reynolds of 200 to 400 and comparatively small change occurring past a Reynolds of 1000. These decreases in average temperature are due to the decrease in residence time of the heat transfer fluid within the pipe. As the Reynolds number increases the fluid spends less time in the pipe resulting in less time for heat to diffuse from the hot stream to the cold stream. PCM activity as shown by the liquid fraction also shows significant differences, as the Reynolds increases the PCM becomes more active with higher peak liquid fractions. Figure 6c,d shows

that an abrupt jump occurs in the liquid fraction from 1000 to 1200 while also changing the overall shape of the pattern seen in the PCM liquid fraction.

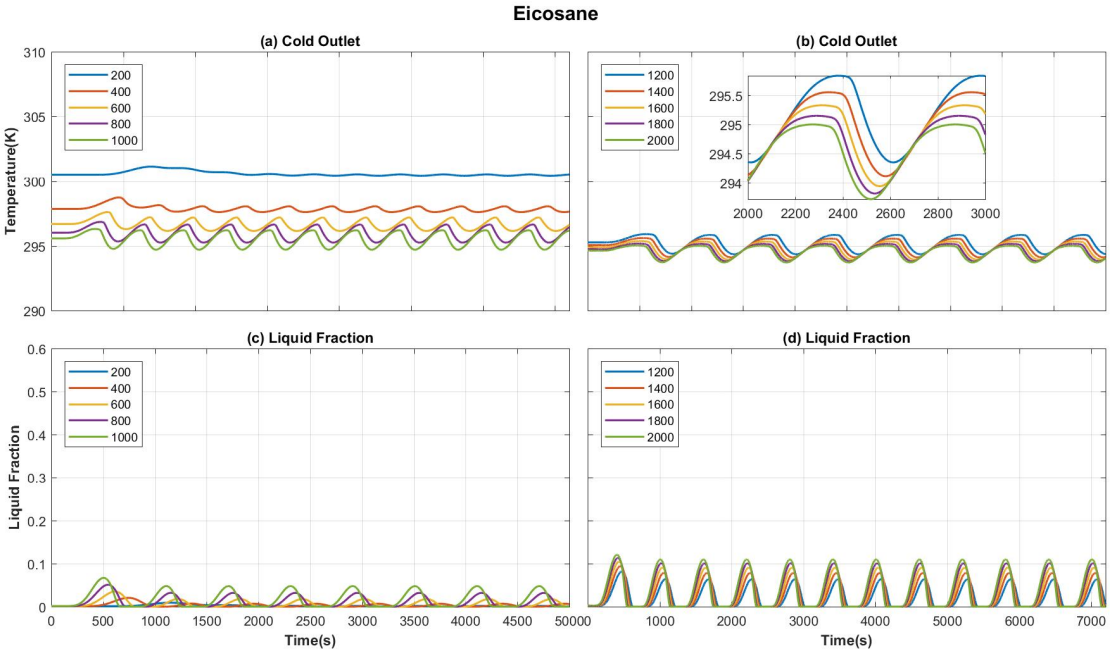

Figure 6. Cold outlet temperature and liquid fraction for eicosane (T_s = 309.35 K, T_l = 310.35 K) at Reynolds from 200 to 2000. Reynolds 200–1000 on the left (**a**,**c**) and 1200–2000 on the right (**b**,**d**). Liquid fractions are shown in (**c**,**d**) show low usage of the PCMs full phase change capacity with (**b**,**d**) showing a trend of lower average temperature of the flow with higher PCM use.

In the case of myristic acid, Figure 7c,d shows that PCM is not active at any Reynolds thus all dampening is due to the sensible heat storage within the PCM. As with the eicosane the average temperature decreases as the Reynolds increases with the largest decrease happening from Reynolds of 200 to 400. The PCM inactivity is attributable to the PCT being only 2K below the maximum temperature of the oscillation. As a result, there is insufficient time for the PCM to absorb sufficient amounts of energy, both sensible and latent, before the inlet temperature once again drops below the PCT. This demonstrates the need to carefully select an appropriate phase change material for the expected temperature oscillations. The overall results still show an appreciable amount of dampening that can be achieved by sensible heat storage, although the overall shape of the variations is unaffected with only the amplitude of the variation showing a decrease.

From the results shown in Figure 8 octadecane provides a very good smoothening effect for the entire range of Reynolds numbers under study. Similar to the previous PCMs the largest jump in average temperature occurs from Reynolds of 200 to 400; however, unlike the other PCMs the octadecane is seen to remain in a partial liquid state during the entire oscillation period due to the PCT being much lower than the other PCMs at 301.65 K. The closeup in Figure 8b shows that small variations still occur within the outlet; however, these remain very consistent across the various Reynolds numbers as seen in the plots as well as in the summary plot in Figure 10 with the major effect being a small decrease in average temperature as the Reynolds number increases.

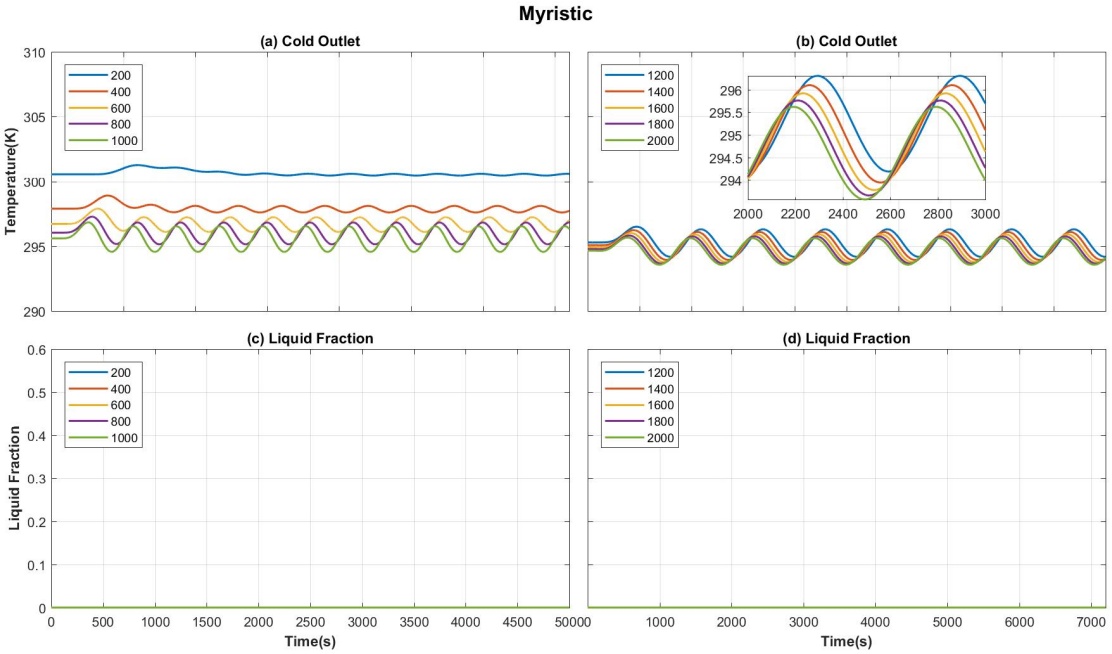

Figure 7. Cold outlet temperature and liquid fraction for myristic acid (T_s = 330.65 K, T_l = 331.65 K) at Reynolds from 200 to 2000. Reynolds 200–1000 on the left (**a**,**c**) and 1200–2000 on the right (**b**,**d**). The PCM is not active as seen in (**c**,**d**), as the material in the PCM layer never reaches the much higher phase change temperature, thus (**a**,**b**) show results for sensible heat storage only.

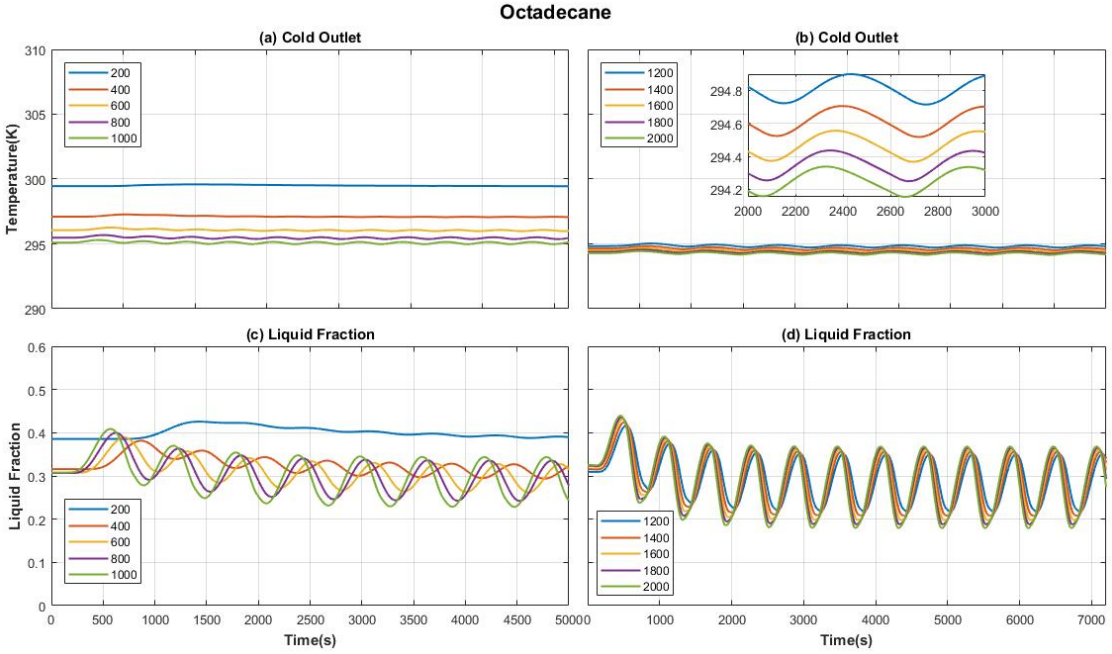

Figure 8. Cold outlet temperature and liquid fraction for octadecane (T_s = 300.65 K, T_l = 301.65 K) at Reynolds from 200 to 2000. Reynolds 200–1000 on the left (**a**,**c**) and 1200–2000 on the right (**b**,**d**). The octadecane remains in a partial phased changed state during the full oscillation cycle. This is reflected in the shape of the cold outlet variations which have a stretched out shape on both the positive and negative variation of the cycle unlike with the eicosane which only shows the structure on the positive component.

Figure 9 show the results for the paraffin wax, similar to all the other PCMs the largest jump in average temperature occurs from Reynolds of 200 to 400 and convergence of the results from Reynolds

of 1000 onwards. PCM activity is very low with small amounts of melting occurring at higher Reynolds number due to a higher PCT of 319.15 K. Overall the results look very similar to those of the myristic acid as most of the dampening is due to sensible heat storage.

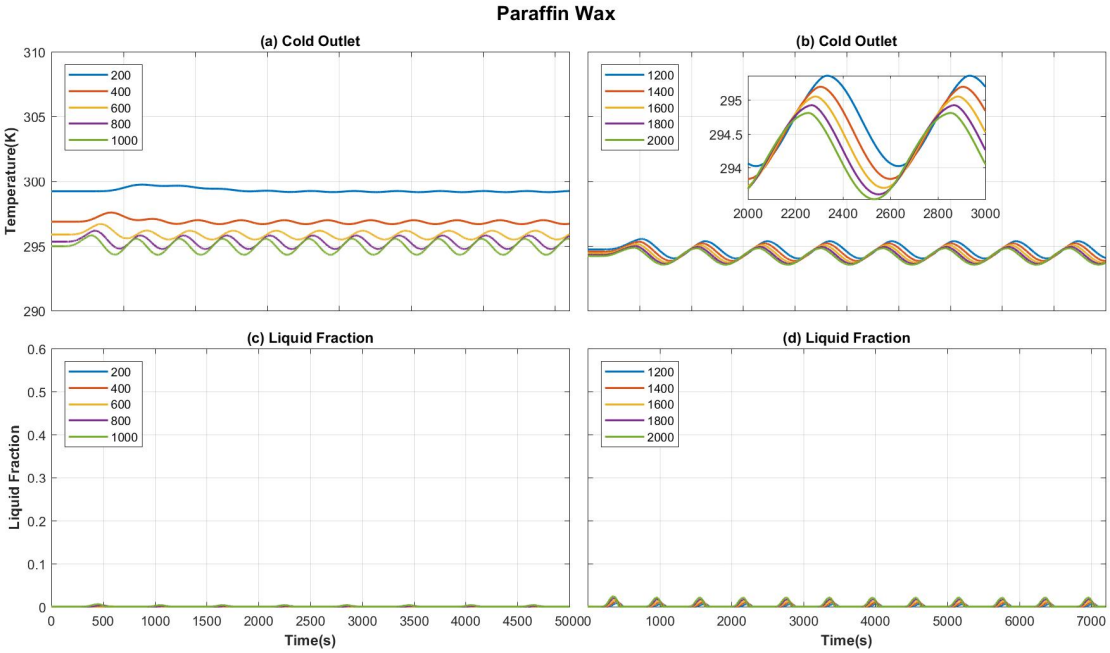

Figure 9. Cold outlet temperature and liquid fraction for paraffin wax (T_s = 319.15 K, T_l = 320.15 K) at Reynolds from 200 to 2000. Reynolds 200–1000 on the left (**a**,**c**) and 1200–2000 on the right (**b**,**d**). The paraffin wax is shown to only phase change a small amount at all Reynolds numbers, the small amounts do not noticeably affect the outlet temperature and the results are very similar to myristic. Despite the phase change temperature being close to the average temperature of the oscillating hot stream, the material is not very active demonstrating the difficulty in selecting an appropriate phase change temperature.

Figure 10 shows the computed average temperatures and ranges of the cold stream outlet for all the PCMs at the various Reynolds numbers. The results are plotted with each line showing the responses of a particular PCM over the range of Reynolds tested. The overall results shown by the figure are in line with what was observed from the previous figures with an overall decrease in outlet temperature with increasing Reynolds number. The oscillation range in general increases as Reynolds increases although with some fluctuation in this trend past Reynolds of 1600, although dampening by octadecane remains fairly consistent above Reynolds 1000.

Overall, several conclusions can be seen from the parametric study of Reynolds numbers and different PCMs. Firstly the behavior of the outlet for any particular PCM shows similar behavior between Reynolds numbers and converges towards a particular behavior once the Reynolds passes 1000. That capacitor performance is tied to the amount of PCM that actively melts and solidifies with more PCM activity generally providing better results. Finally, it is concluded the PCM capacitor can provide dampening through a variety of flow ranges at the cost of reduced heat transfer between the streams. The overall numerical results from the previous section are further summarized in Table 7 which reports the average outlet temperature and oscillation range more precisely than the graphs in Figure 10.

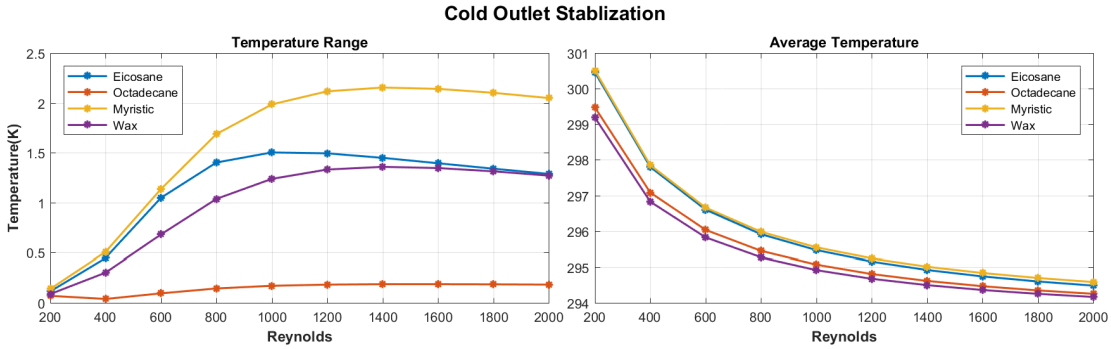

Figure 10. Average temperature and oscillation range for the cold stream outlet as a function of Reynolds number and phase change material. As Reynolds increases a general trend in decrease of the average temperature is seen due to decreased residence time within the pipe. Oscillations also become larger as heat transfer rates increase with no change in the amount of thermal mass being engaged. In the case of eicosane, more material phase changes at higher Reynolds which causes the oscillations to dampen.

Table 7. Range and Average temperature for the cold outlet of the PCM capacitors at different Reynolds numbers.

Cold Stream Outlet Average Temperature (K)				
Reynolds	**Eicosane**	**Myristic**	**Octadecane**	**Wax**
200	300.46	300.52	299.48	299.19
400	297.80	297.85	297.08	296.82
600	296.60	296.66	296.03	295.82
800	295.91	295.98	295.44	295.27
1000	295.46	295.54	295.07	294.91
1200	295.15	295.24	294.81	294.67
1400	294.92	295.01	294.61	294.49
1600	294.74	294.84	294.46	294.36
1800	294.60	294.70	294.35	294.25
2000	294.48	294.58	294.25	294.16
Cold Stream Outlet Temperature Range (K)				
Reynolds	**Eicosane**	**Myristic**	**Octadecane**	**Wax**
200	0.11	0.14	0.07	0.09
400	0.45	0.51	0.04	0.30
600	1.05	1.14	0.09	0.68
800	1.40	1.69	0.14	1.04
1000	1.50	1.99	0.17	1.24
1200	1.49	2.12	0.18	1.33
1400	1.45	2.15	0.19	1.36
1600	1.39	2.14	0.19	1.35
1800	1.34	2.10	0.18	1.31
2000	1.29	2.05	0.18	1.27

4.4. Variation in Frequency and Amplitude

A parametric study was conducted on the base case, varying the period and amplitude of the temperature oscillation to study their effects on the dampening. Results are shown for each of the PCMs below with Figures 11–14 showing the cold outlet temperature when the amplitude is changed from the base case of 20 K to 10 K (low amplitude) and 30 K (high amplitude) as well as when the period is changed from 10 min to 5 min (ow period) and 20 min (high period).

From Figure 11 it can be seen that the range of oscillation is reduced at a lower temperature amplitude and is higher at high amplitude by approximately 0.5 K with the shape of oscillation

changing in both cases, becoming more sinusoidal when the amplitude is decreased and sharper when the amplitude is increased. The range of the oscillation was calculated to have increased by 38% and decreased by 45% for the high and low amplitude cases. As the temperature is increased and decreased the driving force of the oscillation changes proportionally. Variations in period caused a significant change in the stabilization effect of the PCM, at the lower period of 5 min the stabilization effect became substantially better with a more constant outlet temperature being apparent, at a period of 20 min the oscillations increased in magnitude to by close to 2 K. Computed values showed that the oscillations increased by 83% for the high period case and decreased by 83% for the low period case. The change in oscillation range is attributable to the diffusion of heat through the PCM. At longer periods the oscillations the PCM is able to internally change temperature enough that the driving temperature gradient is more apparent, the action of the latent heat can be seen at the maximum of the oscillation as a flattened top. Phase change is keeping the temperature fixed at the transition temperature thus dampening the top end of the oscillation.

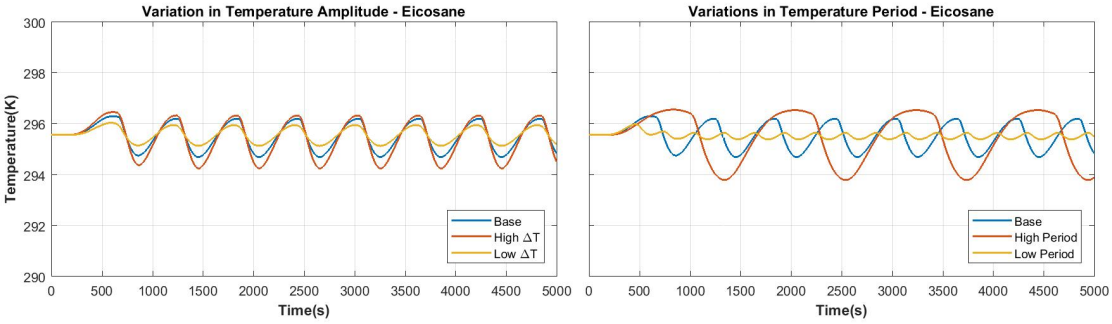

Figure 11. Results of eicosane at Re = 1000 with amplitudes of 10, 20, 30 K and periods of 5, 10, 20 min. Variations due to amplitude differences are seen to be clipped at the maximum at the same point even with higher temperature variations. Higher period oscillations allow for higher max temperature with more pronounced clipping.

From Figure 12 it can be seen that as amplitude increases and decrease so does the outlet temperature variations in a uniform way as only the sensible heat portion of the PCM storage is available for stabilization. As with the eicosane the variations decrease when the period is decreased, and increase when the period is increased; however, the oscillations remain very sinusoidal and regular in all cases. In all cases no latent heat storage is engage as the temperature in the PCM never reaches the phase change temperature of the myristic acid. As a result the curves remain sinusoidal with no reduction at the peaks, thus acting no different than any other sensible storage medium. Overall, myristic showed a 94% increase in variation at the high period case and 50% for the high amplitude case while seeing a decrease in variation of 50% for the low amplitude case and 85% reduction for the low period case.

Figure 13 show the results for octadecane which previously showed the best dampening effect out of the four PCMs evaluated. The effect of changing amplitude is noticeably different for octadecane with a higher amplitude resulting in a lower outlet temperature and a lower amplitude producing a similar range of oscillation to that of the base case. This is possibly attributable to the higher liquid fraction of the PCM at higher amplitudes, as more of the latent heat portion of the PCM is engaged the average thermal conductivity of the layer drops leading to slightly less heat transfer. The effects of changing period are in line with what is seen in the other PCMs with an increase in dampening by 49% at the lower temperature amplitude and an increase in 38% for the higher amplitude. Unlike the other cases, the increase in period resulted in a 262% increase in oscillation while the decrease in period resulted in a 92% reduction in oscillation. The effects of changing periods are in line with what is seen in the other PCMs with a shorter period resulting in higher dampening compared to a longer period resulting in a higher temperature range.

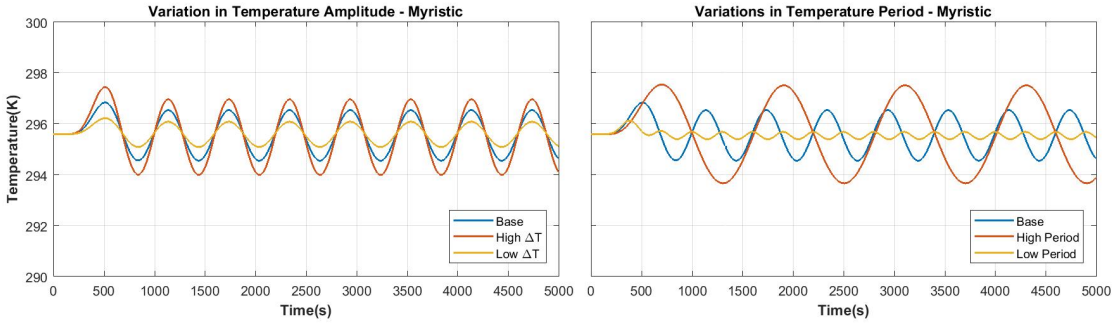

Figure 12. Results of myristic acid at Re = 1000 with amplitudes of 10, 20, 30 K and periods of 5, 10, 20 min. No phase change occurs even with the higher oscillation range and thus the wave simply is scaled. Higher and lower periods result in stretched out and compressed oscillations with higher maximums due to longer diffusion times.

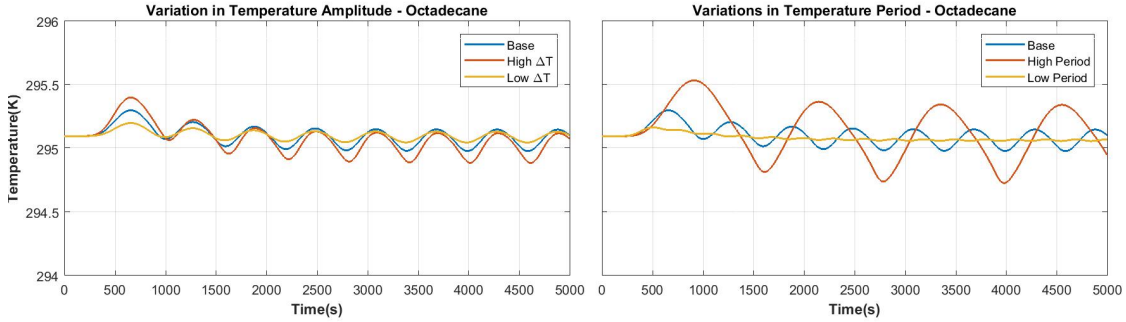

Figure 13. Results of N-octadecane at Re = 1000 with amplitudes of 10, 20, 30 K and periods of 5, 10, 20 min. Octadecane remains at all times in a semi-phase changed state, when the oscillation range is increased the top end of the temperature variations remain similar due to the constant temperature phase change. The high period case showed very constant PCM activity, whereas the low period case showed very rapid swings in PCM use. In all cases the absolute change in oscillation remains small with oscillations less than 1 K.

In the case of the paraffin wax, Figure 14 shows that the temperature range increased by 51% as amplitude increased and decreased 50% as amplitude decreased. Response to the change in period was similar to the previous PCMs, where a decrease in period provided 88% more dampening and an increase in period lead to a 113% increase in oscillation.

Overall, except for the octadecane, the PCMs all showed better performance when the period decreased and when the amplitude of the variation of the hot side inlet decreased. In the case of octadecane, the presence of complete phase change of the capacitor and very good base performance suggests that a higher liquid fraction provides better thermal stabilization. The results of the parametric study show that the dampening effect can cope with changes in the oscillation characteristics and that quick oscillations are better dampened than very slow oscillations.

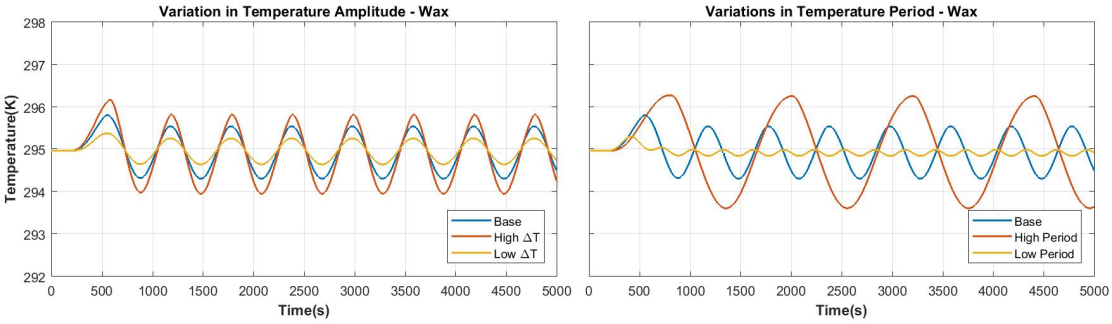

Figure 14. Results of paraffin wax at Re = 1000 with amplitudes of 10, 20, 30 K and periods of 5, 10, 20 min. When the temperature oscillations increase the PCM becomes slightly active which results in slightly lower peak temperature. In the case of variations in period, longer periods did not result in phase change of the material thus more heat diffused through the material due to the longer period at a high temperature in a fashion similar to the myristic acid.

5. Conclusions

A numerical investigation on the performance of a PCM-based thermal capacitor for heat transfer applications was conducted. The results show the ability of a PCM to act as a thermal capacitor with the ability to smooth out variations in the outlet temperature from the exchanger subject to an oscillating input. It was found that a PCM with a lower melting temperature provided better temperature stabilization and that total heat transfer was reduced when PCMs were added. A study of the effect of Reynolds number was conducted and showed that as Reynolds increased, the average temperature decreased substantially while the stabilization effect decreased marginally. Additional study showed that increasing and decreasing the amplitude of the fluctuations caused the outlet temperature to increase and decrease except for the case where there was high PCM activity. Increasing and decreasing the oscillation period showed a significant effect on the outlet oscillation, with a shorter period producing a much smaller range of outlet temperature and a longer period producing noticeably larger variations. It was concluded that the overall benefit of the addition of the PCM are a result of keeping the temperature fixed during the phase change process thus reducing the driving temperature difference. This affect was shown to be prominent in cases where more of the phase change material was engaged as it allowed for more stable thermal gradients. Finally, more studies are required to investigate methods to increase the average temperature of the outlet while maintaining the dampening effect on thermal fluctuations.

Author Contributions: Conceptualization, J.K. and M.F.; methodology, J.K. and M.F.; software, M.F.; validation, J.K.; formal analysis, M.F.; investigation, J.K.; resources, A.P.S.; data curation, M.F. and A.S.; writing—original draft preparation, M.F. and J.K.; writing—review and editing, M.F.; visualization, M.F.; supervision, A.P.S.; project administration, A.P.S.; funding acquisition, A.P.S. All authors have read and agreed to the published version of the manuscript.

Funding: The authors thank the Ultra Deep Mining Network (UDMN) (241695 Tri-Council (NCE—UDMN) 2-003). The simulations were conducted at McGill HPC facility under Calcul-Quebec and Compute-Canada with contribution from CFI-JELF. The first author gratefully acknowledged McGill Engineering Undergraduate Student Masters Award (MEUSMA) and Fonds de recherche du Québec—Nature et technologies (FRQNT)—Bourses de maitrise (B1X) for supporting this research.

Conflicts of Interest: The authors declare no conflict of interest.

Nomenclature

C_m	Mushy constant (kg/(s m^3))
c_p	Specific heat capacity (J/(K kg))
h	Specific enthalpy (J/kg)
ΔH	Latent heat of fusion (J/kg)
k	Thermal conductivity (W/(mK))
p	Pressure (Pa)
T	Temperature (K)
t	Time (s)
$\mathbf{U}$	Velocity (m/s)
D	Diameter (m)
Greek Letter	
γ	Liquid fraction
μ	Viscosity [m^2/s]
ρ	Density [kg/m^3]
τ	Oscillation Period [s]
Superscripts	
T	Transpose
Subscripts	
htf	Heat Transfer Fluid
ℓ	PCM in Liquid Phase
s	PCM in Solid Phase
i	Inner pipe wall
m	Middle pipe wall
o	Outer pipe wall
in	Inlet
out	Outlet
h	Hot
c	Cold

References

1. Li, D.; Ding, Y.; Wang, P.; Wang, S.; Yao, H.; Wang, J.; Huang, Y. Integrating two-stage phase change material thermal storage for cascaded waste heat recovery of diesel-engine-powered distributed generation systems: A case study. *Energies* **2019**, *12*, 2121. [CrossRef]
2. Dal Magro, F.; Meneghetti, A.; Nardin, G.; Savino, S. Enhancing energy recovery in the steel industry: Matching continuous charge with off-gas variability smoothing. *Energy Convers. Manag.* **2015**, *104*, 78–89. [CrossRef]
3. Sun, W.; Hong, Y.; Wang, Y. Operation optimization of steam accumulators as thermal energy storage and buffer units. *Energies* **2017**, *10*, 17. [CrossRef]
4. Mazzucco, G.; Xotta, G.; Salomoni, V.A.; Giannuzzi, M.; Maiorana, C.E. Solid thermal storage with PCM materials. Numerical investigations. *Appl. Therm. Eng.* **2017**, *124*, 545–559. [CrossRef]
5. Jaguemont, J.; Omar, N.; Van den Bossche, P.; Mierlo, J. Phase-change materials (PCM) for automotive applications: A review. *Appl. Therm. Eng.* **2018**, *132*, 308–320. [CrossRef]
6. Verdier, D.; Ferrière, A.; Falcoz, Q.; Siros, F.; Couturier, R. Experimentation of a High Temperature Thermal Energy Storage Prototype Using Phase Change Materials for the Thermal Protection of a Pressurized Air Solar Receiver. *Energy Procedia* **2014**, *49*, 1044–1053. [CrossRef]
7. Nardin, G.; Meneghetti, A.; Dal Magro, F.; Benedetti, N. PCM-based energy recovery from electric arc furnaces. *Appl. Energy* **2014**, *136*, 947–955. [CrossRef]
8. Dal Magro, F.; Benasciutti, D.; Nardin, G. Thermal stress analysis of PCM containers for temperature smoothing of waste gas. *Appl. Therm. Eng.* **2016**, *106*, 1010–1022. [CrossRef]
9. Dal Magro, F.; Savino, S.; Meneghetti, A.; Nardin, G. Coupling waste heat extraction by phase change materials with superheated steam generation in the steel industry. *Energy* **2017**, *137*, 1107–1118. [CrossRef]

10. Alawadhi, E.M. Temperature regulator unit for fluid flow in a channel using phase change material. *Appl. Therm. Eng.* **2005**, *25*, 435–449. [CrossRef]
11. Charvat, P.; Stetina, J.; Pech, O.; Klimes, L.; Ostry, M. Experimental investigation of stabilization of flowing water temperature with a water-PCM heat exchanger. *EPJ Web Conf.* **2014**, *67*, 02046. [CrossRef]
12. Charvat, P.; Klimes, L.; Stetina, J.; Ostry, M. Thermal storage as a way to attenuate fluid-temperature fluctuations: Sensible-heat versus latent-heat storage materials. *Mater. Technol.* **2014**, *48*, 423–427.
13. Kurnia, J.C.; Sasmito, A.P. Numerical investigation of phase change materials thermal capacitor for pipe flow. *MATEC Web Conf.* **2017**, *131*, 01001. [CrossRef]
14. Nascimento Porto, T.; Delgado, J.M.P.Q.; Guimaraes, A.S.; Fernandes Magalhaes, H.L.; Moreira, G.; Brito Correia, B.; Freire de Andrade, T.; Barbosa de Lima, A.G. Phase Change Material Melting Process in a Thermal Energy Storage System for Applications in Buildings. *Energies* **2020**, *13*, 3254.10.3390/en13123254. [CrossRef]
15. Kurnia, J.C.; Sasmito, A.P. Numerical investigation of heat transfer performance of a rotating latent heat thermal energy storage. *Appl. Energy* **2018**, *227*, 542–554. [CrossRef]
16. Kurnia, J.C.; Sasmito, A.P.; Ping, S.I. Investigation of Heat Transfer on a Rotating Latent Heat Energy Storage. *Energy Procedia* **2017**, *105*, 4173–4178. [CrossRef]
17. Kurnia, J.C.; Sasmito, A.P.; Jangam, S.V.; Mujumdar, A.S. Improved design for heat transfer performance of a novel phase change material (PCM) thermal energy storage (TES). *Appl. Therm. Eng.* **2013**, *50*, 896–907. [CrossRef]
18. Kurnia, J.C.; Sasmito, A.P.; Mujumdar, A.S. Numerical investigation of laminar heat transfer performance of various cooling channel designs. *Appl. Therm. Eng.* **2011**, *31*, 1293–1304. [CrossRef]
19. Kays, W.M.; Crawford, M.E.; Weigand, B. *Convective Heat and Mass Transfer*, 4th ed.; McGraw-Hill Series in Mechanical Engineering; McGraw-Hill Higher Education: Boston, MA, USA, 2005.
20. Hale, D.; Hoover, M.; O'Neill, M. *Phase Change Materials Handbook*; National Technical Information Service U.S. Department of Commerce: Washington, DC, USA, 1971.
21. Lacroix, M. Numerical simulation of a shell-and-tube latent heat thermal energy storage unit. *Sol. Energy* **1993**, *50*, 357–367. [CrossRef]

© 2020 by the authors. Licensee MDPI, Basel, Switzerland. This article is an open access article distributed under the terms and conditions of the Creative Commons Attribution (CC BY) license (http://creativecommons.org/licenses/by/4.0/).